TURBULENT SKIN-FRICTION DRAG REDUCTION BY SPANWISE WALL OSCILLATION WITH GENERIC TEMPORAL WAVEFORM

Andrea Cimarelli
DIN
University of Bologna
Via Fontanelle, 40, 47121 Forlì, Italy
andrea.cimarelli2@unibo.it

Bettina Frohnapfel
Institute of Fluid Mechanics
Karlsruhe Institute of Technology
Kaiserstr. 10, 76131 Karlsruhe, Germany
bettina.frohnapfel@kit.edu

Yosuke Hasegawa
Institute of Industrial Science
The University of Tokyo
4-6-1 Komaba, Meguro-ku, Tokyo 153-8505, Japan
ysk@iis.u-tokyo.ac.jp

Elisabetta De Angelis
DIN
University of Bologna
Via Fontanelle, 40, 47121 Forlì, Italy
e.deangelis@unibo.it

Maurizio Quadrio
Department of Aerospace Science and Technologies
Politecnico di Milano
Campus La Masa, 20156 Milano, Italy
maurizio.quadrio@polimi.it

ABSTRACT

To generalize the well-known spanwise-oscillating-wall technique for drag reduction, non-sinusoidal oscillations of a solid wall are considered as a means to alter the skin-friction drag in a turbulent channel flow. A series of Direct Numerical Simulations is conducted to evaluate the control performance of nine different waveforms, in addition to the usual sinusoid, systematically changing the maximum wave amplitude and the period for each waveform.

The turbulent average spanwise motion is found to coincide with the laminar Stokes solution that can be constructed, for the generic waveform, through harmonic superposition. A newly defined penetration depth of the Stokes layer is then used to build a simple tool that allows predicting turbulent drag reduction and net energy saving rate for any waveform.

Among all the cases considered, the sinusoid at optimal amplitude and period is found to yield the maximum net energy saving rate. However, when the wave amplitude and period deviate from the optimal values, other waves are found to perform better than the sinusoid. This is potentially interesting in view of applications, where a particular actuator limitations might preclude reaching the optimal operating conditions for the sinusoidal wall oscillation. It is demonstrated that the present model can predict the locally optimal waveform for given wave amplitude and period, as well as the globally optimal sinusoidal wave.

INTRODUCTION

The efficient use of energy in systems where a relative motion between a solid wall and a fluid takes place is perhaps the most important driving factor that supports the current research effort into aerodynamic drag reduction.

We consider here skin-friction turbulent drag. Existing open-loop techniques provide higher drag reduction than passive methods while being less complex than feedback-control methods. In particular, open-loop techniques that rely on the spanwise forcing of the near-wall turbulent flow have been shown to yield large drag reduction and interestingly positive energy budgets in numerical simulations (Quadrio, 2011), and first laboratory experiments have already been carried out (Auteri *et al.*, 2010; Gouder, 2011; Choi *et al.*, 2011). The present paper deals with the simplest and well-known spanwise oscillating-wall technique.

Most existing open-loop control strategies assume a sinusoidal waveform as control input. On the other hand, when trying to verify these control strategies in experiments, various constraints are placed on the properties of a control input by the used actuators. Hence, it is of key importance to identify the optimal waveform to achieve best control performance: this is the aim of the present paper.

As a starting point, we select a set of waveforms and comparatively study, via several numerical experiments, how the drag-reduction and energetic performances of the oscillating wall depend on the waveform as well as on the oscillation amplitude and period. Guided by our numerical experiments, we then aim at obtaining results of more general validity, so that a predictive tool for the control performance of non-sinusoidal wall oscillations can eventually be developed. In this process, we take advantage of the laminar solution that exists for the spanwise flow alone (the Stokes oscillating boundary layer), by extending it to a generic (periodic) temporal waveform.

THE NUMERICAL EXPERIMENTS

The performance of non-sinusoidal spanwise wall oscillations is assessed using Direct Numerical Simulation (DNS) of a turbulent channel flow. Discretization is spectral (Fourier) in the homogeneous x and z directions, whereas compact, explicit fourth-order finite differences are used in the wall-normal y direction. Time advancement is carried out with a partially implicit, third-order Crank–Nicholson/Runge–Kutta scheme.

The Reynolds number of the reference simulation without wall oscillation is $Re = U_b h/\nu = 3173$, where U_b is the bulk velocity, h is half the channel gap and ν is the kinematic viscosity of the fluid. This corresponds to a value of the friction-based Reynolds number $Re_\tau = 200$. Unless otherwise specified, h and U_b are chosen as length and velocity scales. The computational domain is $9.6h \times 2h \times 4.8h$ along x, y and z directions, with $192 \times 128 \times 192$ grid points / modes respectively. Every simulation is started from the same initial condition of fully developed turbulent channel flow without wall oscillation. When the wall moves, drag reduction takes place. Since the flow rate is kept constant, the space-averaged streamwise pressure gradient and the friction drag decrease. The total integration time for each simulation is 95 wash-out time units, where the wash-out time unit is defined as L_x/U_b. This value corresponds to $10,000$ viscous time units. After the beginning of the oscillating movement of the walls at $t = 0$, a certain time interval is needed for the flow to reach the new equilibrium state. Time average is hence started only after the initial transient of the flow, by simply discarding the first 25% of the entire time integration interval.

Various waveforms of the temporal oscillation of the wall are examined. We consider spanwise wall velocities $W_w(t)$ varying in time as

$$W_w(t) = W_m f_\alpha\left(\frac{t}{T}\right), \qquad (1)$$

where f_α (with $\alpha = a, \ldots, j$) are ten periodic functions of unit period with values ranging from -1 to 1. All the considered oscillations thus have period T and amplitude W_m. It is worth mentioning that, as Quadrio & Ricco (2004) pointed out, in flow control with wall oscillation, a third parameter besides oscillation period and amplitude enters the picture, i.e. the maximum displacement of the wall during the oscillation cycle. If the wall oscillates sinusoidally in time, however, only two of these three parameters are truly independent, and the maximum displacement can be easily deduced once period and amplitude are known. Hence, considering different waveforms, we can open up the third dimension in the parameters space, and investigate the behavior of the oscillating wall when the temporal waveform is considered as a free parameter, and the constraint of sinusoidal oscillation is lifted. The maximum displacement of the wall from the reference position during the oscillation cycle is

$$D_m = 2\int_0^{T/2} W_w(t)dt. \qquad (2)$$

The first waveform f_a is the usual sinusoid

$$W_w(t) = W_m \sin\left(2\pi\frac{t}{T}\right) \qquad (3)$$

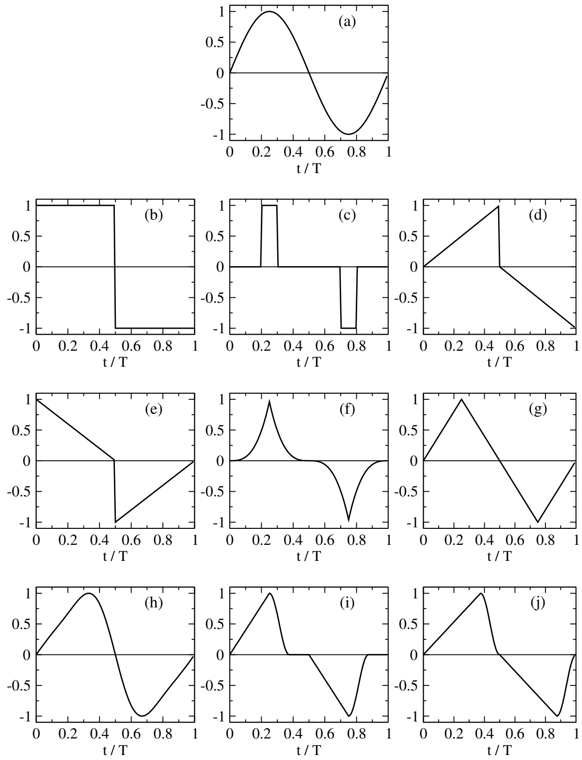

Figure 1. Temporal waveforms of the wall oscillation considered in the present work. The following symbols are used throughout the paper for the different waveforms: (a) ($\triangle$), (b) ($\blacklozenge$), (c) ($*$), (d) ($+$), (e) ($\blacksquare$), (f) ($\bullet$), (g) ($\blacktriangleleft$), (h) ($\blacktriangleright$), (i) ($\blacktriangle$) and (j) ($\blacktriangledown$).

for which $D_m = 2W_m T/\pi$. The other waveforms are sketched in figure 1 (additional waveforms have been considered in this work but are not discussed here). Despite all the possible choices, the periodic functions f_α which have been included in this study have been chosen as being representative of the different features which may characterize non-sinusoidal oscillations in practice. The waveforms f_α allow for discontinuities in velocity and acceleration, large and small accelerations, phase shifts and different fractions of the period with constant velocity and even zero velocity.

For each waveform, the oscillation parameters W_m and T are varied around the values T_0^+ and $W_{m,0}^+$ (the superscript $+$ as customary implies non-dimensionalization in viscous units, where the velocity scale is the friction velocity u_τ of the reference flow) that yield the maximum net efficiency for the sinusoid. This particular condition was carefully determined by Quadrio & Ricco (2004) and corresponds to $T_0^+ = 125$ and $W_{m,0}^+ = 4.5$. We consider a parametric set of variations from this basic case, by changing W_m^+ and T^+ to values twice and one half of the optimal value.

FLOW CONTROL PERFORMANCE

The performance of the oscillating wall as a flow control technique is analyzed following Kasagi *et al.* (2009) in terms of three dimensionless indicators: the drag reduction rate R, the power input due to the applied control, P_{in} and the net energy saving rate, $S = R - P_{in}$.

Figure 2 describes how R, P_{in} and S are affected by non-sinusoidal temporal waveforms, for two of the tested waveforms. Notwithstanding the marked quantitative dif-

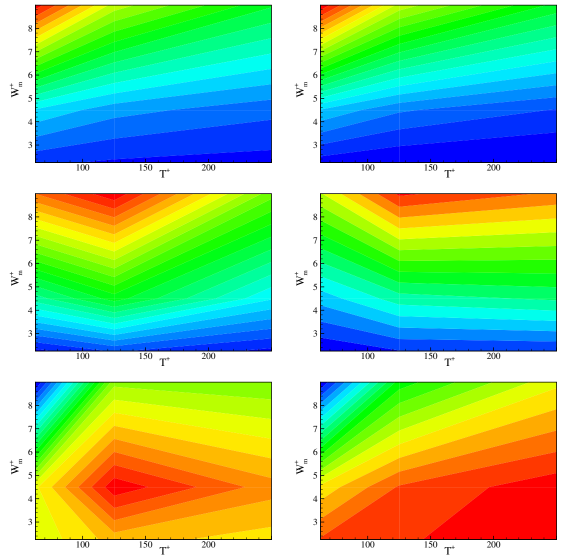

Figure 2. Power consumption rate P_{in} (top), reduction of pumping power R (center), and net energy saving S (bottom) as a function of W_m^+ and T^+ for two selected waveforms, (c) and (g), see figure 1 for reference. The color coding goes from maximum values, red, to minimum values, blue.

ferences among the considered waveforms, both P_{in} and R qualitatively behave in the (T, W_m)-space like the one reported in Quadrio & Ricco (2004) for the sinusoidal case. The power consumption P_{in} for each value of T increases with W_m. For constant W_m, P_{in} decreases with increasing T. The drag reduction rate, R, always presents its maximum at the intermediate period $T^+ = 125$, and it increases monotonically with increasing W_m. Overall, the specific waveform f_α enters the picture by affecting the quantitative values of P_{in} and R. For example, waveform (b) (not shown) leads to much larger P_{in} than the sinusoid while yielding a larger R than the sinusoid. However, the increase in P_{in} outweighs the one in R such that the net saving, S, is reduced in comparison to the sinusoid. Decreasing values for P_{in} and R are observed for the cusp-like waveform (f) which also results in a worse S compared to the sinusoid. In fact, all the considered waveforms yield a best S which is smaller than the S obtained with sinusoidal oscillations at the optimal conditions $T_0^+ = 125$ and $W_{m0}^+ = 4.5$, i.e. $S_0 = 0.078$. For nearly all cases considered the balance between R and P_{in} is such that $S > 0$ at low W_m, whereas at larger W_m higher values of R but even larger values of P_{in} are obtained, such that S is reduced. In general, most of the waveforms show a maximum of S at intermediate values of (T, W_m) which are close to those of the sinusoidal case.

GENERALIZED WAVEFORM

The alternating boundary layer that is created by a sinusoidally oscillating wall in a quiescent fluid is described by the solution of the so-called Stokes' second problem (Schlichting & Gersten, 2000). It has been shown that this solution also describes well the spanwise component of a turbulent channel flow modified by the oscillating wall, when properly averaged in space and considered as a function of the oscillation phase. Moreover the analytical expression $w_{St}(y,t)$ of the laminar Stokes layer has proven useful for the prediction of practically important quantities, like P_{in} and R, for turbulent flows over oscillating walls (provided that the oscillating period does not largely exceed its optimal value). The equivalence between $w_{St}(y,t)$ and the space-mean, phase-averaged turbulent profile $\langle w \rangle(y,\tau)$, first found for the pipe flow by Quadrio & Sibilla (2000), implies that the spanwise space-averaged momentum equation reduces to a diffusion equation analogous to that of the laminar Stokes problem, i.e.

$$\frac{\partial w}{\partial t} = \frac{1}{Re}\frac{\partial^2 w}{\partial y^2}, \tag{4}$$

and the Reynolds stress term $\partial \langle w'v' \rangle / \partial y$ is negligible (Ricco & Quadrio, 2008).

Our preliminary step becomes that of verifying whether this property applies to the general, non-sinusoidal case too, since it might help interpreting and generalizing the results reported in the previous section. Since Eq. (4) is linear, the obvious starting point is to consider a harmonic decomposition of the waveform, and to build the solution as linear superposition of the various Stokes components. For a single sinusoidal mode, i.e. the sinusoidal oscillation (3), the analytical Stokes solution for laminar flows reads

$$w_{St}(y,t) = W_m \mathrm{e}^{-y/\delta} \sin\left(\frac{2\pi}{T}t - \frac{y}{\delta}\right) \tag{5}$$

where the wall-normal lengthscale δ is defined as

$$\delta = \sqrt{\frac{T}{\pi Re}}. \tag{6}$$

In the general case, the time-dependent boundary condition (1) for the diffusion equation (4) can be expressed via the following Fourier series

$$W_w(t) = W_m \sum_{n=1}^{+\infty} A_n \mathrm{e}^{j(2\pi n/T)t} + c.c. \tag{7}$$

where j is the imaginary unit, A_n is the complex coefficient of the n-th Fourier component and $c.c.$ stands for complex conjugate. The resulting expression for the waveform-generalized spanwise Stokes layer, obtained by superposition of the elementary solutions, reads as

$$w_{St}(y,t) = W_m \sum_{n=1}^{+\infty} A_n \mathrm{e}^{-\sqrt{n}y/\delta} \mathrm{e}^{j[(2\pi n/T)t - \sqrt{n}y/\delta]} + c.c.. \tag{8}$$

Figure 3 demonstrates the close agreement between the laminar solution expressed by the superposition (8) and the turbulent space-averaged profile for a non-sinusoidal waveform. It should be noted that the figure plots the turbulent profiles for waveform (f), that most significantly deviates from the sinusoid, to emphasize how Eq.(8) provides a rather robust description of the transverse boundary layer created by the wall movement. The knowledge of the spanwise velocity profile can now be exploited to derive a predictive tool for the assessment of the control performance for wall oscillations of arbitrary waveform. This is described in the following.

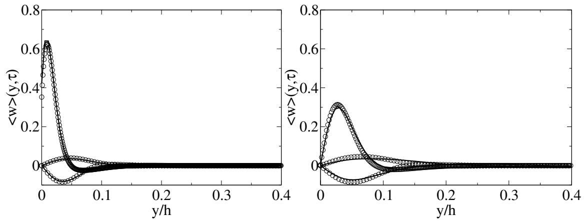

Figure 3. Comparison between the laminar solution expressed by Eq. 8 (symbols), with summation truncated at 128 coefficients, and the turbulent averaged spanwise velocity, $\langle w \rangle(y,\tau)$ at different oscillation phases for waveform (f) (lines). Left: (T_0, W_{m0}). Right: $(2T_0, W_{m0})$.

PREDICTION OF CONTROL PERFORMANCE

The input power required by the sinusoidal oscillation is written analytically via the Stokes' solution (5), and reads

$$\mathscr{P}_{in} = \frac{W_m^2}{2}\sqrt{\frac{\pi}{TRe}}. \tag{9}$$

Normalization of this quantity with the time-averaged pumping power per unit channel wall area in the fixed-wall case corresponds to the performance indicator P_{in} introduced above. For a generic waveform, expressed through the Fourier series (7), the same quantity becomes

$$\mathscr{P}_{in} = W_m^2\sqrt{\frac{\pi}{TRe}}\sum_{n=1}^{+\infty} 2|A_n|^2\sqrt{n}. \tag{10}$$

As shown in Fig. 4 (top left), the power consumption computed with Eq. (10) is in excellent agreement with the simulation results for the entire dataset. The inset highlights how the percentage error remains small even when the absolute value of P_{in} approaches zero. Eq. (10) can thus be used to predict P_{in} for arbitrary values of T and W_m, as well as for arbitrary waveforms. Moreover, the same equation highlights that $\mathscr{P}_{in} \propto W_m^2\sqrt{\pi/ReT}$ such that the qualitative dependency of P_{in} on T and W_m is independent of the waveform, as already observed in figure 2.

The prediction of the turbulent drag reduction rate R is much less trivial, since R does not simply derive from the laminar solution (8) but results from the complex non-linear interaction between the oscillation of the wall and near-wall turbulence. Nonetheless, several proposals are available in the literature to link properties of the transverse layer with R. In particular, it has been suggested, for example by Choi *et al.* (2002) and Quadrio & Ricco (2004), that R scales with a parameter that combines a length and an acceleration scale of the spanwise alternating layer.

The wall-normal length scale, $\tilde{\ell}$, is related to the penetration of the Stokes layer into the channel, and is defined as the largest distance from the wall where the maximum wall-induced spanwise velocity exceeds a threshold velocity, W_{th}. For the sinusoidal waveform, the analytical solution (5) yields

$$\tilde{\ell}(W_{th}) = \delta \ln\left(\frac{W_m}{W_{th}}\right), \tag{11}$$

where δ is defined by (6).

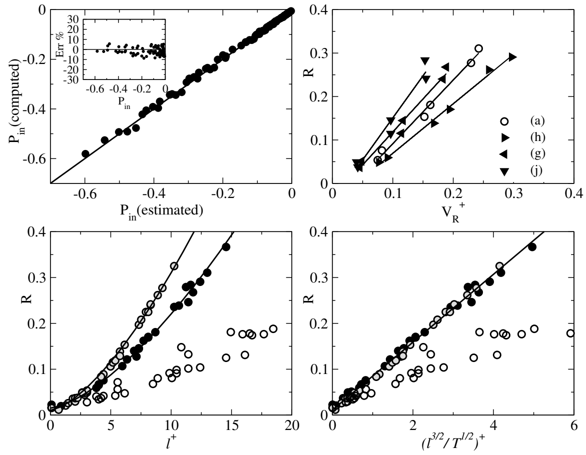

Figure 4. Top plots. Left: power consumption data P_{in} for all the simulations considered in this work versus the analytical prediction based on the Stokes layer assumption, equation (10). The inset plot shows the precentage error of the predictions. Right: drag reduction rate, R, for four selected waveforms for $T^+ \leq 150$ versus the parameter V_R^+ numerically computed from equation 8 for $y^+ = 6.3$ and $W_{th}^+ = 1.2$. Bottom plots. Left: turbulent drag reduction R as a function of penetration depth ℓ^+, with ℓ computed from Eq. (15) using a threshold $\sigma_{th}^+ = 0.8$ corresponding to the intensity of spanwise turbulent fluctuations in the uncontrolled case at $y^+ \approx 9$. Gray symbols are for $T^+ = 62.5$, black symbols for $T^+ = 125$ and open symbols for $T^+ = 250$. Lines are a fit with the power law $\ell^{3/2}$. Right: same data, plotted versus $\ell^{3/2}T^{-1/2}$, following Eq. (16).

The acceleration scale is a local maximum spanwise acceleration, a_m, induced by the Stokes layer in a position close to the wall. For the sinusoidal waveform, the analytical solution (5) yields

$$a_m(y) = \frac{2\pi}{T} W_m \mathrm{e}^{-y/\delta}.$$

These two quantities have been grouped together by Choi *et al.* (2002) to form a scaling parameter that reads

$$V_R(y, W_{th}) = \frac{a_m(y)\tilde{\ell}(W_{th})}{W_m} = 2\sqrt{\frac{\pi}{TRe}}\ln\left(\frac{W_m}{W_{th}}\right)\mathrm{e}^{-y/\delta}. \tag{12}$$

This scaling parameter, evaluated for $y^+ = 6.3$ and $W_{th}^+ = 1.2$, is known (Quadrio & Ricco, 2004; Touber & Leschziner, 2012) to scale linearly with R, provided that $T^+ \leq 150$.

Unfortunately, this scaling parameter does not work for non-sinusoidal waveforms. Figure 4 (top right) shows that the present data for $T^+ \leq 150$ versus the parameter V_R do not collapse into a single curve.

In order to find a universal scaling parameter for the drag reduction rate achieved with different waveforms, the relation between R and the laminar Stokes layer thickness is revisited. For the sinusoidal case the Stokes layer thickness increases with W_m and scales with $\sqrt{T/Re}$ (see Eq. (5) and the definition of δ). For the generic waveform, the same dependence holds for every harmonic component. However, the generalized expression (8) reveals a phase shift among

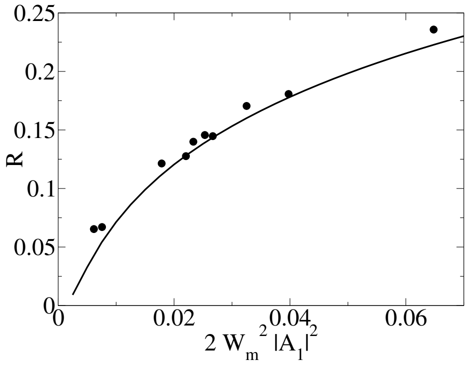

Figure 5. Turbulent drag reduction rate, R, as a function of $2W_m^2|A_1|^2$ for $T^+ = 125$. The continuous line is the prediction (16), with ℓ computed from the first mode only, equation (18).

the various harmonic components, so that the correct velocity scale to define the penetration depth cannot simply be W_m anymore. A good candidate for the definition of an effective penetration length for non-sinusoidal oscillations is the mean square value (variance) of the oscillating spanwise velocity, $\overline{w_{St}(y,t)^2}$, which for the sinusoidal case reads

$$\overline{w_{St}^2}(y) = \frac{W_m^2}{2} e^{-2y/\delta}. \tag{13}$$

In analogy to the classical penetration length of the Stokes layer, $\tilde{\ell}$, a new penetration length, ℓ, can thus be defined as the distance from the wall where the induced variance of the velocity drops below a certain threshold value σ_{th}^2. The previous Eq. (13) thus yields for the sinusoid

$$\ell(\sigma_{th}) = \frac{1}{2}\delta \ln\left(\frac{W_m^2}{2\sigma_{th}^2}\right). \tag{14}$$

For the generic waveform, the variance of the oscillating velocity is given by

$$\overline{w_{St}^2}(y) = W_m^2 \sum_{n=1}^{\infty} 2|A_n|^2 e^{-2\sqrt{n}y/\delta}, \tag{15}$$

and this highlights how each mode contributes to the variance with a weighing factor which decays exponentially with increasing n. This observation is important for the following derivations. We also remark that, in general, the penetration length, ℓ, cannot be expressed analytically, but must be computed numerically from Eq. (15). In computing ℓ, the value $W_{th}^+ = 1.2$ is converted into the equivalent $\sigma_{th}^+ = 0.8$ which follows form Eq.(14) for the sinusoidal waveform.

Figure 4 (bottom left) shows that the relationship between R and ℓ is indeed similar for all the different waveforms considered. As already remarked by several authors, for cases with large oscillation periods drag reduction drops and the interaction between the streamwise turbulent flow and the slowly oscillating Stokes layer changes nature and trivially becomes a cyclic reorientation of the former by the latter. In figure 4 (bottom) the same graphical representation as employed by Quadrio & Ricco (2011) is adopted,

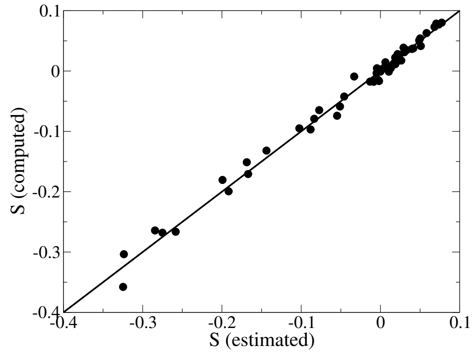

Figure 6. Measured net energy saving data S versus its estimate through the Stokes layer thickness ℓ computed from Eq. (16) and the analytical prediction of power consumption, Eq. (10). The inset plots all data at $T^+ \leq 150$, whereas the main plot is a zoom in the region $S > 0$.

and the data corresponding to slow oscillations are plotted with open symbols.

For a given forcing period at $T^+ < 150$ (i.e. for datasets represented with black- and gray-filled symbols), data for all the waveforms collapse onto one line, well fitted by a power law $\sim \ell^{3/2}$. As shown in figure 4 (bottom right), a linear scaling is obtained when R is plotted against $\ell^{3/2}T^{-1/2}$ where $T^{-1/2}$, as in Eq. (12), accounts for the physical process of diffusion. The term $T^{-1/2}$ carries the relevant contribution of the acceleration term a_m in the expression (12) for V_R, which however is affected not only by T but also by the harmonic distribution in the waveform. Neglecting the latter dependency upon the specific waveform yields the correct scaling parameter that is valid for any waveform.

Hence, the turbulent drag reduction rate is well predicted by the expression

$$R = h_1 \ell^{+(3/2)} T^{+(-1/2)} + h_2 \tag{16}$$

where h_1 and h_2 are coefficients for which a linear fit of the present data at $Re_\tau = 200$ and $T^+ < 150$ yields $h_1 = 0.0738$ and $h_2 = 0.02$. As expected, the proposed scaling is indeed not valid for $T^+ > 150$.

The strong link between the penetration length ℓ and the drag reduction R for $T^+ < 150$ can be further exploited to provide an analytical *a priori* estimate of the drag reduction capabilities of a generic waveform, when W_m and T are given. Owing to the n modulation, the sum in (15) can be approximated with its first term as

$$\sum_{n=1}^{+\infty} 2|A_n|^2 e^{-2\sqrt{n}y/\delta} \simeq 2|A_1|^2 e^{-2y/\delta}. \tag{17}$$

This approximation allows for an analytical estimate of ℓ as

$$\ell(\sigma_{th}) = \frac{1}{2}\delta \ln\left(\frac{2W_m^2|A_1|^2}{\sigma_{th}^2}\right). \tag{18}$$

By plugging actual numerical values of the spectral components in (15), one can easily realize that for the second Fourier component to produce a contribution to the

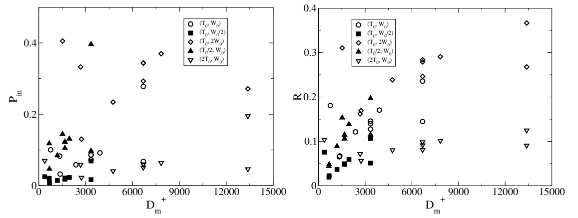

Figure 7. Dependency of the power consumption rate P_{in} (left) and reduction of friction power R (right) on the maximum displacement D^+_m for five different pairs of (T, W_m).

variance comparable to the first one, it must be $|A_2|/|A_1| \sim 10$. Since for the waveforms considered in the present work the first mode happens to be by far the most energetic, approximation (17) is reasonable. In a waveform where the first mode is not dominant, the spectrum should increase with n at least exponentially; in such a case, this would bring about a dramatic increase of the power consumption and would make such a waveform highly unpractical.

The estimation of R is now possible analytically using Eq. (16) when ℓ is computed through (18), i.e. using only its first Fourier harmonic. This estimation of R is included in figure 5 as a solid line, and shows very good agreement with the data points obtained by DNS.

Since P_{in} and also R have been shown to be predictable purely on the basis of the laminar solution of the Stokes layer the net energy saving rate, S, can also be predicted. Figure 6 shows that the prediction quality for S is high throughout the entire range of available data, and that the scatter remains very limited in the most interesting narrow region where $S > 0$. Such predictive capabilities are obviously useful since the required solutions of equations (10) and (15) do not require extensive computations. Hence, the present predictive tool can be used to guide the design of the wall movement when trying to realize an oscillating wall in practice. Lastly, let us remark that the present approach is naturally also valid for the classical sinusoidal oscillation, of which it represents a generalization.

In closing, let us briefly discuss the dependency of the overall performance, S, in terms of P_{in} and R, on the maximum displacement D_m for the different waveforms. Let us recall that from the geometrical point of view the value of the maximum displacement is proportion to the area under the curves in Fig. 1 hence the plots of the S vs. D_m, where in turn T^+ and W^+_m are kept constant, will resemble the plots of Fig. 2, respectively. More precisely, one single plot would be spread in turns in each direction accordingly to the proportionality constants due to the different shapes. Indeed our approach allows to study the effect of D_m independently on the period and the maximum oscillation through the waveforms. Namely given the definition (2) it is possible to reconstruct the dependence of D_m on the spectral distribution as

$$D_m = 2\int_0^{T/2} \left[W_m \sum_{n=1}^{+\infty} A_n e^{j(2\pi n/T)t} + c.c. \right] dt. \qquad (19)$$

This approach yields the expression

$$D_m = 2W_m T \left[\sum_{n=1}^{+\infty} A_n \frac{p_n}{2\pi n} + c.c. \right] \qquad (20)$$

where p_n is a complex coefficient which results from the integration of the Fourier polynomials and is independent on the waveforms. Equation (20), once compared with equations (10) and (15) for P_{in} and $\overline{w^2_{St}}(y)$ respectively, clearly shows that the spectral distribution of the different waveforms influences in completely different ways these three observables. Namely, an infinite number of waveforms, corresponding to different sets of coefficients A_n, can lead to the same displacement. Parallely, waveforms characterized by the same P_{in} or R, and hence by the same S, can have completely different values of D_m.

This lack of correlation between the maximum displacement and P_{in}, R and S is verified by the present data as shown in Fig. 7.

CONCLUSION

In short, it is found that the waveform actually matters, and that the sinusoidal waveform is the best when one is interested in the net energy saving. However, what is true for the absolute optimum in parameter space is not true anymore locally, so that for certain combinations of oscillation periods and amplitudes temporal waveforms exist that outperform the sinusoid.

REFERENCES

Auteri, F., Baron, A., Belan, M., Campanardi, G. & Quadrio, M. 2010 Experimental assessment of drag reduction by traveling waves in a turbulent pipe flow. *Phys. Fluids* **22** (11), 115103/14.

Choi, J.-I., Xu, C.-X. & Sung, H. J. 2002 Drag reduction by spanwise wall oscillation in wall-bounded turbulent flows. *AIAA J.* **40** (5), 842–850.

Choi, K.-S., Jukes, T. & Whalley, R. 2011 Turbulent boundary-layer control with plasma actuators. *Phil. Trans. R. Soc. A* **369** (1940), 1443–1458.

Gouder, K. 2011 Turbulent Friction Drag Reduction Using Electroactive Polymer Surfaces. PhD thesis, Imperical College, London.

Kasagi, N., Hasegawa, Y. & Fukagata, K. 2009 Towards cost-effective control of wall turbulence for skin-friction drag reduction. *Advances in Turbulence XII*, vol. 132, pp. 189–200. Springer.

Quadrio, M. 2011 Drag reduction in turbulent boundary layers by in-plane wall motion. *Phil. Trans. R. Soc. A* **369** (1940), 1428–1442.

Quadrio, M. & Ricco, P. 2004 Critical assessment of turbulent drag reduction through spanwise wall oscillation. *J. Fluid Mech.* **521**, 251–271.

Quadrio, M. & Ricco, P. 2011 The laminar generalized Stokes layer and turbulent drag reduction. *J. Fluid Mech.* **667**, 135–157.

Quadrio, M. & Sibilla, S. 2000 Numerical simulation of turbulent flow in a pipe oscillating around its axis. *J. Fluid Mech.* **424**, 217–241.

Ricco, P. & Quadrio, M. 2008 Wall-oscillation conditions for drag reduction in turbulent channel flow. *Intl J. Heat Fluid Flow* **29**, 601–612.

Schlichting, H. & Gersten, K. 2000 *Boundary-Layer Theory*. Springer, Berlin.

Touber, E. & Leschziner, M.A. 2012 Near-wall streak modification by spanwise oscillatory wall motion and drag-reduction mechanisms. *J. Fluid Mech.* **693**, 150–200.